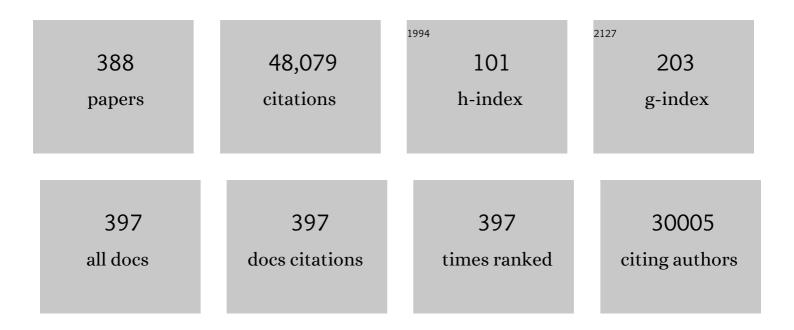
Peter C M Van Zijl

List of Publications by Year in descending order

Source: https://exaly.com/author-pdf/7040003/publications.pdf Version: 2024-02-01



#	Article	IF	CITATIONS
1	Three-dimensional tracking of axonal projections in the brain by magnetic resonance imaging. Annals of Neurology, 1999, 45, 265-269.	5.3	3,317
2	Fiber tracking: principles and strategies – a technical review. NMR in Biomedicine, 2002, 15, 468-480.	2.8	1,859
3	Fiber Tract–based Atlas of Human White Matter Anatomy. Radiology, 2004, 230, 77-87.	7.3	1,727
4	Stereotaxic white matter atlas based on diffusion tensor imaging in an ICBM template. NeuroImage, 2008, 40, 570-582.	4.2	1,528
5	Reproducibility of quantitative tractography methods applied to cerebral white matter. NeuroImage, 2007, 36, 630-644.	4.2	1,464
6	Tract probability maps in stereotaxic spaces: Analyses of white matter anatomy and tract-specific quantification. NeuroImage, 2008, 39, 336-347.	4.2	1,293
7	Using the amide proton signals of intracellular proteins and peptides to detect pH effects in MRI. Nature Medicine, 2003, 9, 1085-1090.	30.7	999
8	Family income, parental education and brain structure in children and adolescents. Nature Neuroscience, 2015, 18, 773-778.	14.8	979
9	DtiStudio: Resource program for diffusion tensor computation and fiber bundle tracking. Computer Methods and Programs in Biomedicine, 2006, 81, 106-116.	4.7	910
10	Chemical exchange saturation transfer (CEST): What is in a name and what isn't?. Magnetic Resonance in Medicine, 2011, 65, 927-948.	3.0	903
11	Determining the longitudinal relaxation time (T1) of blood at 3.0 Tesla. Magnetic Resonance in Medicine, 2004, 52, 679-682.	3.0	594
12	Water saturation shift referencing (WASSR) for chemical exchange saturation transfer (CEST) experiments. Magnetic Resonance in Medicine, 2009, 61, 1441-1450.	3.0	555
13	Amide proton transfer (APT) contrast for imaging of brain tumors. Magnetic Resonance in Medicine, 2003, 50, 1120-1126.	3.0	544
14	Imaging cortical association tracts in the human brain using diffusionâ€ŧensorâ€based axonal tracking. Magnetic Resonance in Medicine, 2002, 47, 215-223.	3.0	534
15	Human brain white matter atlas: Identification and assignment of common anatomical structures in superficial white matter. NeuroImage, 2008, 43, 447-457.	4.2	486
16	Diffusion Tensor Imaging and Axonal Tracking in the Human Brainstem. NeuroImage, 2001, 14, 723-735.	4.2	484
17	Quantitative assessment of blood flow, blood volume and blood oxygenation effects in functional magnetic resonance imaging. Nature Medicine, 1998, 4, 159-167.	30.7	461
18	Atlas-based whole brain white matter analysis using large deformation diffeomorphic metric mapping: Application to normal elderly and Alzheimer's disease participants. NeuroImage, 2009, 46, 486-499.	4.2	456

#	Article	IF	CITATIONS
19	Differentiation between glioma and radiation necrosis using molecular magnetic resonance imaging of endogenous proteins and peptides. Nature Medicine, 2011, 17, 130-134.	30.7	448
20	Functional magnetic resonance imaging based on changes in vascular space occupancy. Magnetic Resonance in Medicine, 2003, 50, 263-274.	3.0	428
21	Chemical exchange saturation transfer imaging and spectroscopy. Progress in Nuclear Magnetic Resonance Spectroscopy, 2006, 48, 109-136.	7.5	415
22	Water diffusion and acute stroke. Magnetic Resonance in Medicine, 1994, 31, 154-163.	3.0	396
23	Pediatric diffusion tensor imaging: Normal database and observation of the white matter maturation in early childhood. NeuroImage, 2006, 29, 493-504.	4.2	383
24	Artificial reporter gene providing MRI contrast based on proton exchange. Nature Biotechnology, 2007, 25, 217-219.	17.5	379
25	Dual-Modality Monitoring of Targeted Intraarterial Delivery of Mesenchymal Stem Cells After Transient Ischemia. Stroke, 2008, 39, 1569-1574.	2.0	371
26	MRI detection of glycogen in vivo by using chemical exchange saturation transfer imaging (glycoCEST). Proceedings of the National Academy of Sciences of the United States of America, 2007, 104, 4359-4364.	7.1	370
27	White and gray matter development in human fetal, newborn and pediatric brains. NeuroImage, 2006, 33, 27-38.	4.2	346
28	Effects of signalâ€ŧoâ€noise ratio on the accuracy and reproducibility of diffusion tensor imaging–derived fractional anisotropy, mean diffusivity, and principal eigenvector measurements at 1.5T. Journal of Magnetic Resonance Imaging, 2007, 26, 756-767.	3.4	336
29	DTI tractography based parcellation of white matter: Application to the mid-sagittal morphology of corpus callosum. NeuroImage, 2005, 26, 195-205.	4.2	335
30	Accurate quantitation of water-amide proton exchange rates using the phase-modulated CLEAN chemical EXchange (CLEANEX-PM) approach with a Fast-HSQC (FHSQC) detection scheme. Journal of Biomolecular NMR, 1998, 11, 221-226.	2.8	324
31	Multi-parametric neuroimaging reproducibility: A 3-T resource study. NeuroImage, 2011, 54, 2854-2866.	4.2	318
32	Amide proton transfer imaging of human brain tumors at 3T. Magnetic Resonance in Medicine, 2006, 56, 585-592.	3.0	308
33	Practical data acquisition method for human brain tumor amide proton transfer (APT) imaging. Magnetic Resonance in Medicine, 2008, 60, 842-849.	3.0	304
34	Optical coherence tomography reflects brain atrophy in multiple sclerosis: A fourâ€year study. Annals of Neurology, 2015, 78, 801-813.	5.3	304
35	Detection of the Ischemic Penumbra Using pH-Weighted MRI. Journal of Cerebral Blood Flow and Metabolism, 2007, 27, 1129-1136.	4.3	296
36	Natural <scp>D</scp> â€glucose as a biodegradable MRI contrast agent for detecting cancer. Magnetic Resonance in Medicine, 2012, 68, 1764-1773.	3.0	295

#	Article	IF	CITATIONS
37	Quantifying exchange rates in chemical exchange saturation transfer agents using the saturation time and saturation power dependencies of the magnetization transfer effect on the magnetic resonance imaging signal (QUEST and QUESP): Ph calibration for poly-L-lysine and a starburst dendrimer. Magnetic Resonance in Medicine, 2006, 55, 836-847.	3.0	288
38	Atlas-guided tract reconstruction for automated and comprehensive examination of the white matter anatomy. NeuroImage, 2010, 52, 1289-1301.	4.2	277
39	Multi-contrast human neonatal brain atlas: Application to normal neonate development analysis. NeuroImage, 2011, 56, 8-20.	4.2	277
40	Routine clinical brain MRI sequences for use at 3.0 Tesla. Journal of Magnetic Resonance Imaging, 2005, 22, 13-22.	3.4	272
41	Diffusion Tensor MR Imaging of the Brain and White Matter Tractography. American Journal of Roentgenology, 2002, 178, 3-16.	2.2	270
42	Nuclear Overhauser enhancement (NOE) imaging in the human brain at 7T. NeuroImage, 2013, 77, 114-124.	4.2	266
43	Quantitative description of proton exchange processes between water and endogenous and exogenous agents for WEX, CEST, and APT experiments. Magnetic Resonance in Medicine, 2004, 51, 945-952.	3.0	258
44	Quantitative proton MR spectroscopic imaging of the human brain. Magnetic Resonance in Medicine, 1996, 35, 356-363.	3.0	254
45	Diffusion Weighting by the Trace of the Diffusion Tensor within a Single Scan. Magnetic Resonance in Medicine, 1995, 33, 41-52.	3.0	243
46	Diffusion tensor imaging of the developing mouse brain. Magnetic Resonance in Medicine, 2001, 46, 18-23.	3.0	237
47	APTâ€weighted MRI: Techniques, current neuro applications, and challenging issues. Journal of Magnetic Resonance Imaging, 2019, 50, 347-364.	3.4	224
48	Magnetization Transfer Contrast and Chemical Exchange Saturation Transfer MRI. Features and analysis of the field-dependent saturation spectrum. NeuroImage, 2018, 168, 222-241.	4.2	220
49	Oxygenation and hematocrit dependence of transverse relaxation rates of blood at 3T. Magnetic Resonance in Medicine, 2007, 58, 592-597.	3.0	216
50	Mechanism of magnetization transfer during on-resonance water saturation. A new approach to detect mobile proteins, peptides, and lipids. Magnetic Resonance in Medicine, 2003, 49, 440-449.	3.0	200
51	Sensitive NMR Detection of Cationic-Polymer-Based Gene Delivery Systems Using Saturation Transfer via Proton Exchange. Journal of the American Chemical Society, 2001, 123, 8628-8629.	13.7	196
52	Developing MR reporter genes: promises and pitfalls. NMR in Biomedicine, 2007, 20, 275-290.	2.8	196
53	Quantitative description of the asymmetry in magnetization transfer effects around the water resonance in the human brain. Magnetic Resonance in Medicine, 2007, 58, 786-793.	3.0	196
54	Multimodal imaging of the self-regulating developing brain. Proceedings of the National Academy of Sciences of the United States of America, 2012, 109, 19620-19625.	7.1	192

#	Article	IF	CITATIONS
55	MRI-detectable pH nanosensors incorporated intoÂhydrogels for inÂvivo sensing of transplanted-cell viability. Nature Materials, 2013, 12, 268-275.	27.5	189
56	New "multicolor―polypeptide diamagnetic chemical exchange saturation transfer (DIACEST) contrast agents for MRI. Magnetic Resonance in Medicine, 2008, 60, 803-812.	3.0	188
57	Threeâ€dimensional amide proton transfer MR imaging of gliomas: Initial experience and comparison with gadolinium enhancement. Journal of Magnetic Resonance Imaging, 2013, 38, 1119-1128.	3.4	181
58	Multi-contrast large deformation diffeomorphic metric mapping for diffusion tensor imaging. NeuroImage, 2009, 47, 618-627.	4.2	179
59	In vivo threeâ€dimensional wholeâ€brain pulsed steadyâ€state chemical exchange saturation transfer at 7 T. Magnetic Resonance in Medicine, 2012, 67, 1579-1589.	3.0	176
60	On the relationship between seedâ€based and ICAâ€based measures of functional connectivity. Magnetic Resonance in Medicine, 2011, 66, 644-657.	3.0	172
61	Analysis of noise effects on DTIâ€based tractography using the bruteâ€force and multiâ€ROI approach. Magnetic Resonance in Medicine, 2004, 52, 559-565.	3.0	169
62	From the diffusion coefficient to the diffusion tensor. NMR in Biomedicine, 2002, 15, 431-434.	2.8	165
63	MR tracking of transplanted cells with "positive contrast―using manganese oxide nanoparticles. Magnetic Resonance in Medicine, 2008, 60, 1-7.	3.0	164
64	Calibration and validation of TRUST MRI for the estimation of cerebral blood oxygenation. Magnetic Resonance in Medicine, 2012, 67, 42-49.	3.0	162
65	Long-term influence of normal variation in neonatal characteristics on human brain development. Proceedings of the National Academy of Sciences of the United States of America, 2012, 109, 20089-20094.	7.1	158
66	Application of Phase-Modulated CLEAN Chemical EXchange Spectroscopy (CLEANEX-PM) to Detect Waterâ^'Protein Proton Exchange and Intermolecular NOEs. Journal of the American Chemical Society, 1997, 119, 6203-6204.	13.7	154
67	Three-dimensional anatomical characterization of the developing mouse brain by diffusion tensor microimaging. NeuroImage, 2003, 20, 1639-1648.	4.2	153
68	Dynamic Glucose-Enhanced (DGE) MRI: Translation to Human Scanning and First Results in Glioma Patients. Tomography, 2015, 1, 105-114.	1.8	153
69	Absolute Quantitation of Diffusion Constants in Human Stroke. Stroke, 1997, 28, 483-490.	2.0	153
70	Sustained Poststimulus Elevation in Cerebral Oxygen Utilization after Vascular Recovery. Journal of Cerebral Blood Flow and Metabolism, 2004, 24, 764-770.	4.3	152
71	Atlas-based analysis of neurodevelopment from infancy to adulthood using diffusion tensor imaging and applications for automated abnormality detection. NeuroImage, 2010, 52, 415-428.	4.2	152
72	Flow Territory Mapping of the Cerebral Arteries With Regional Perfusion MRI. Stroke, 2004, 35, 882-887.	2.0	150

#	Article	IF	CITATIONS
73	DeepHarmony: A deep learning approach to contrast harmonization across scanner changes. Magnetic Resonance Imaging, 2019, 64, 160-170.	1.8	150
74	Spatial normalization of diffusion tensor fields. Magnetic Resonance in Medicine, 2003, 50, 175-182.	3.0	143
75	Theoretical and experimental investigation of the VASO contrast mechanism. Magnetic Resonance in Medicine, 2006, 56, 1261-1273.	3.0	142
76	Association of Cortical Lesion Burden on 7-T Magnetic Resonance Imaging With Cognition and Disability in Multiple Sclerosis. JAMA Neurology, 2015, 72, 1004.	9.0	140
77	On the precision of diffusion/perfusion imaging by gradient sensitization. Magnetic Resonance in Medicine, 1992, 23, 122-129.	3.0	138
78	Human brain atlas for automated region of interest selection in quantitative susceptibility mapping: Application to determine iron content in deep gray matter structures. NeuroImage, 2013, 82, 449-469.	4.2	138
79	Orientation-independent diffusion imaging without tensor diagonalization: Anisotropy definitions based on physical attributes of the diffusion ellipsoid. Journal of Magnetic Resonance Imaging, 1999, 9, 804-813.	3.4	135
80	Regional white matter change in pre-symptomatic Huntington's disease: A diffusion tensor imaging study. Psychiatry Research - Neuroimaging, 2005, 140, 55-62.	1.8	135
81	Fast 3D chemical exchange saturation transfer (CEST) imaging of the human brain. Magnetic Resonance in Medicine, 2010, 64, 638-644.	3.0	134
82	Proton MR Spectroscopic and Diffusion Tensor Brain MR Imaging in X-linked Adrenoleukodystrophy: Initial Experience. Radiology, 2002, 225, 245-252.	7.3	133
83	Applying amide proton transferâ€weighted MRI to distinguish pseudoprogression from true progression in malignant gliomas. Journal of Magnetic Resonance Imaging, 2016, 44, 456-462.	3.4	132
84	Gradient-enhanced HMQC and HSQC spectroscopy. Applications to 15N-labeled Mnt repressor. Journal of the American Chemical Society, 1991, 113, 9688-9690.	13.7	128
85	Restricted and anisotropic displacement of water in healthy cat brain and in stroke studied by NMR diffusion imaging. Magnetic Resonance in Medicine, 1991, 19, 327-332.	3.0	128
86	Multislice proton magnetic resonance spectroscopic imaging in X-linked adrenoleukodystrophy. Annals of Neurology, 1994, 36, 595-608.	5.3	126
87	A Framework for Callosal Fiber Distribution Analysis. NeuroImage, 2002, 17, 1131-1143.	4.2	126
88	Predicting IDH mutation status in grade II gliomas using amide proton transferâ€weighted (APTw) MRI. Magnetic Resonance in Medicine, 2017, 78, 1100-1109.	3.0	126
89	Simplified quantitative description of amide proton transfer (APT) imaging during acute ischemia. Magnetic Resonance in Medicine, 2007, 57, 405-410.	3.0	122
90	Functional Analysis of Aquaporin-1 Deficient Red Cells. Journal of Biological Chemistry, 1996, 271, 1309-1313.	3.4	119

#	Article	IF	CITATIONS
91	Sensitive CEST agents based on nucleic acid imino proton exchange: Detection of poly(rU) and of a dendrimer-poly(rU) model for nucleic acid delivery and pharmacology. Magnetic Resonance in Medicine, 2003, 49, 998-1005.	3.0	117
92	Variable delay multi-pulse train for fast chemical exchange saturation transfer and relayed-nuclear overhauser enhancement MRI. Magnetic Resonance in Medicine, 2014, 71, 1798-1812.	3.0	115
93	Measurement of tissue oxygen extraction ratios from venous bloodT2: Increased precision and validation of principle. Magnetic Resonance in Medicine, 2001, 46, 282-291.	3.0	112
94	Sickle Cell Disease: Continuous Arterial Spin-labeling Perfusion MR Imaging in Children. Radiology, 2003, 227, 567-574.	7.3	111
95	Intracellular volume and apparent diffusion constants of perfused cancer cell cultures, as measured by NMR. Magnetic Resonance in Medicine, 1997, 37, 825-832.	3.0	109
96	In vivo visualization of human neural pathways by magnetic resonance imaging. Annals of Neurology, 2000, 47, 412-414.	5.3	109
97	MRI Reporter Genes. Journal of Nuclear Medicine, 2008, 49, 1905-1908.	5.0	109
98	Quantitative Susceptibility Mapping Suggests Altered Brain Iron in Premanifest Huntington Disease. American Journal of Neuroradiology, 2016, 37, 789-796.	2.4	107
99	Proton NMR spectroscopy of solvent-saturable resonances: A new approach to study pH effectsin Situ. Magnetic Resonance in Medicine, 1998, 40, 36-42.	3.0	106
100	Two-Compartment Exchange Model for Perfusion Quantification Using Arterial Spin Tagging. Journal of Cerebral Blood Flow and Metabolism, 2001, 21, 440-455.	4.3	106
101	Novel approach to the measurement of absolute cerebral blood volume using vascular-space-occupancy magnetic resonance imaging. Magnetic Resonance in Medicine, 2005, 54, 1403-1411.	3.0	105
102	In vivo multicolor molecular MR imaging using diamagnetic chemical exchange saturation transfer liposomes. Magnetic Resonance in Medicine, 2012, 67, 1106-1113.	3.0	104
103	Imaging the physiological evolution of the ischemic penumbra in acute ischemic stroke. Journal of Cerebral Blood Flow and Metabolism, 2018, 38, 1500-1516.	4.3	104
104	Identifying Recurrent Malignant Glioma after Treatment Using Amide Proton Transfer-Weighted MR Imaging: A Validation Study with Image-Guided Stereotactic Biopsy. Clinical Cancer Research, 2019, 25, 552-561.	7.0	104
105	Experimental measurement of extravascular parenchymal BOLD effects and tissue oxygen extraction fractions using multi-echo VASO fMRI at 1.5 and 3.0 T. Magnetic Resonance in Medicine, 2005, 53, 808-816.	3.0	103
106	Highâ€ŧhroughput screening of chemical exchange saturation transfer MR contrast agents. Contrast Media and Molecular Imaging, 2010, 5, 162-170.	0.8	103
107	A motion correction scheme by twin-echo navigation for diffusion-weighted magnetic resonance imaging with multiple RF echo acquisition. Magnetic Resonance in Medicine, 1998, 40, 511-516.	3.0	102
108	Impaired cortico-striatal functional connectivity in prodromal Huntington's Disease. Neuroscience Letters, 2012, 514, 204-209.	2.1	101

#	Article	IF	CITATIONS
109	Venous blood effects in spin-echo fMRI of human brain. Magnetic Resonance in Medicine, 1999, 42, 617-626.	3.0	100
110	In Vivo proton spectroscopy and spectroscopic imaging of {1-13C}-g1ucose and its metabolic products. Magnetic Resonance in Medicine, 1993, 30, 544-551.	3.0	98
111	Detrimental effects of BOLD signal in arterial spin labeling fMRI at high field strength. Magnetic Resonance in Medicine, 2006, 56, 546-552.	3.0	97
112	Reproducibility and Temporal Structure in Weekly Resting-State fMRI over a Period of 3.5 Years. PLoS ONE, 2015, 10, e0140134.	2.5	97
113	Determination of Oxygen Extraction Ratios by Magnetic Resonance Imaging. Journal of Cerebral Blood Flow and Metabolism, 1999, 19, 1289-1295.	4.3	95
114	fMRI evidence for multisensory recruitment associated with rapid eye movements during sleep. Human Brain Mapping, 2009, 30, 1705-1722.	3.6	95
115	Dynamic glucose enhanced (DGE) MRI for combined imaging of blood-brain barrier break down and increased blood volume in brain cancer. Magnetic Resonance in Medicine, 2015, 74, 1556-1563.	3.0	94
116	Correction of B0 susceptibility induced distortion in diffusion-weighted images using large-deformation diffeomorphic metric mapping. Magnetic Resonance Imaging, 2008, 26, 1294-1302.	1.8	93
117	Amide proton transfer imaging of 9L gliosarcoma and human glioblastoma xenografts. NMR in Biomedicine, 2008, 21, 489-497.	2.8	92
118	Mapping magnetic susceptibility anisotropies of white matter in vivo in the human brain at 7T. NeuroImage, 2012, 62, 314-330.	4.2	92
119	Measuring Random Microscopic Motion of Water in Tissues with MR Imaging. Journal of Computer Assisted Tomography, 1991, 15, 19-25.	0.9	91
120	Three-Dimensional Diffusion Tensor Magnetic Resonance Microimaging of Adult Mouse Brain and Hippocampus. NeuroImage, 2002, 15, 892-901.	4.2	91
121	An account of the discrepancy between MRI and PET cerebral blood flow measures. A high-field MRI investigation. NMR in Biomedicine, 2006, 19, 1043-1054.	2.8	91
122	Wholeâ€brain amide proton transfer (APT) and nuclear overhauser enhancement (NOE) imaging in glioma patients using lowâ€power steadyâ€state pulsed chemical exchange saturation transfer (CEST) imaging at 7T. Journal of Magnetic Resonance Imaging, 2016, 44, 41-50.	3.4	91
123	Water Exchange Filter with Improved Sensitivity (WEX II) to Study Solvent-Exchangeable Protons. Application to the Consensus Zinc Finger Peptide CP-1. Journal of Magnetic Resonance Series B, 1996, 110, 96-101.	1.6	88
124	Automated fiber tracking of human brain white matter using diffusion tensor imaging. NeuroImage, 2008, 42, 771-777.	4.2	87
125	High-resolution diffusion tensor imaging of the brain stem at 3 T. American Journal of Neuroradiology, 2004, 25, 1325-30.	2.4	87
126	Invivo nmr diffusion spectroscopy:31p application to phosphorus metabolites in muscle. Magnetic Resonance in Medicine. 1990. 13. 467-477.	3.0	86

#	Article	IF	CITATIONS
127	Short Echo Time Proton MR Spectroscopic Imaging. Journal of Computer Assisted Tomography, 1993, 17, 1-14.	0.9	86
128	Multiparametric magnetic resonance imaging analysis of the corticospinal tract in multiple sclerosisâ~†. NeuroImage, 2007, 38, 271-279.	4.2	84
129	Noninvasive Detection of Cerebral Hypoperfusion and Reversible Ischemia from Reductions in the Magnetic Resonance Imaging Relaxation Time, T2. Journal of Cerebral Blood Flow and Metabolism, 1998, 18, 911-920.	4.3	83
130	Detection of amyloid plaques in mouse models of Alzheimer's disease by magnetic resonance imaging. Magnetic Resonance in Medicine, 2004, 51, 452-457.	3.0	83
131	Evidence of slow maturation of the superior longitudinal fasciculus in early childhood by diffusion tensor imaging. NeuroImage, 2007, 38, 239-247.	4.2	83
132	High bâ€value qâ€space diffusionâ€weighted MRI of the human cervical spinal cord in vivo: Feasibility and application to multiple sclerosis. Magnetic Resonance in Medicine, 2008, 59, 1079-1089.	3.0	83
133	Monitoring Enzyme Activity Using a Diamagnetic Chemical Exchange Saturation Transfer Magnetic Resonance Imaging Contrast Agent. Journal of the American Chemical Society, 2011, 133, 16326-16329.	13.7	83
134	In vivo high-resolution diffusion tensor imaging of the mouse brain. Neurolmage, 2013, 83, 18-26.	4.2	83
135	NMR of partially aligned liquids: magnetic susceptibility anisotropies and dielectric properties. Accounts of Chemical Research, 1984, 17, 172-180.	15.6	81
136	Mapping postnatal mouse brain development with diffusion tensor microimaging. NeuroImage, 2005, 26, 1042-1051.	4.2	81
137	Transforming Thymidine into a Magnetic Resonance Imaging Probe for Monitoring Gene Expression. Journal of the American Chemical Society, 2013, 135, 1617-1624.	13.7	80
138	Indirect Detection of Labile Solute Proton Spectra via the Water Signal Using Frequency-Labeled Exchange (FLEX) Transfer. Journal of the American Chemical Society, 2010, 132, 1813-1815.	13.7	79
139	Magnetic susceptibility contrast variations in multiple sclerosis lesions. Journal of Magnetic Resonance Imaging, 2016, 43, 463-473.	3.4	79
140	Review and consensus recommendations on clinical <scp>APT</scp> â€weighted imaging approaches at <scp>3T</scp> : Application to brain tumors. Magnetic Resonance in Medicine, 2022, 88, 546-574.	3.0	79
141	Quantitative proton MR spectroscopic imaging of normal human cerebellum and brain stem. Magnetic Resonance in Medicine, 2001, 46, 699-705.	3.0	78
142	The BOLD post-stimulus undershoot, one of the most debated issues in fMRI. NeuroImage, 2012, 62, 1092-1102.	4.2	76
143	Label-free CEST MRI Detection of Citicoline-Liposome Drug Delivery in Ischemic Stroke. Theranostics, 2016, 6, 1588-1600.	10.0	74
144	Improving the detection sensitivity of p <scp>H</scp> â€weighted amide proton transfer <scp>MRI</scp> in acute stroke patients using extrapolated semisolid magnetization transfer reference signals. Magnetic Resonance in Medicine, 2017, 78, 871-880.	3.0	74

#	Article	IF	CITATIONS
145	Separation of intramolecular NOE and exchange peaks in water exchange spectroscopy using spin-echo filters. Journal of Biomolecular NMR, 1996, 7, 77-82.	2.8	73
146	Defining an Acidosis-Based Ischemic Penumbra from pH-Weighted MRI. Translational Stroke Research, 2012, 3, 76-83.	4.2	73
147	Lesion Heterogeneity on High-Field Susceptibility MRI Is Associated with Multiple Sclerosis Severity. American Journal of Neuroradiology, 2016, 37, 1447-1453.	2.4	73
148	Correlation of the Average Water Diffusion Constant with Cerebral Blood Flow and Ischemic Damage after Transient Middle Cerebral Artery Occlusion in Cats. Journal of Cerebral Blood Flow and Metabolism, 1996, 16, 881-891.	4.3	72
149	Magnetization transfer contrast–suppressed imaging of amide proton transfer and relayed nuclear overhauser enhancement chemical exchange saturation transfer effects in the human brain at 7T. Magnetic Resonance in Medicine, 2016, 75, 88-96.	3.0	72
150	Individual differences in frontolimbic circuitry and anxiety emerge with adolescent changes in endocannabinoid signaling across species. Proceedings of the National Academy of Sciences of the United States of America, 2016, 113, 4500-4505.	7.1	72
151	Blood oxygenation levelâ€dependent (BOLD) total and extravascular signal changes and Δ <i>R</i> ₂ * in human visual cortex at 1.5, 3.0 and 7.0 T. NMR in Biomedicine, 2011, 24, 25-34.	2.8	71
152	Brain metabolite alterations and cognitive dysfunction in early Huntington's disease. Movement Disorders, 2012, 27, 895-902.	3.9	71
153	Simultaneous detection and separation of hyperacute intracerebral hemorrhage and cerebral ischemia using amide proton transfer MRI. Magnetic Resonance in Medicine, 2015, 74, 42-50.	3.0	71
154	Single ¹⁹ F Probe for Simultaneous Detection of Multiple Metal Ions Using miCEST MRI. Journal of the American Chemical Society, 2015, 137, 78-81.	13.7	70
155	Brain iron deficiency in idiopathic restless legs syndrome measured by quantitative magnetic susceptibility at 7 tesla. Sleep Medicine, 2016, 22, 75-82.	1.6	70
156	Quantitative magnetic resonance imaging assessment of cerebral ischemia in rat using on-resonance T1 in the rotating frame. Magnetic Resonance in Medicine, 1999, 42, 268-276.	3.0	69
157	Natural Dâ€glucose as a biodegradable MRI relaxation agent. Magnetic Resonance in Medicine, 2014, 72, 823-828.	3.0	69
158	Prefrontal Brain Network Connectivity Indicates Degree of Both Schizophrenia Risk and Cognitive Dysfunction. Schizophrenia Bulletin, 2014, 40, 653-664.	4.3	69
159	Creatine and phosphocreatine mapping of mouse skeletal muscle by a polynomial and Lorentzian lineâ€shape fitting CEST method. Magnetic Resonance in Medicine, 2019, 81, 69-78.	3.0	69
160	Multiparametric MRI correlates of sensorimotor function in the spinal cord in multiple sclerosis. Multiple Sclerosis Journal, 2013, 19, 427-435.	3.0	68
161	Measurement of <i>T</i> ₁ and <i>T</i> ₂ in the cervical spinal cord at 3 tesla. Magnetic Resonance in Medicine, 2008, 60, 213-219.	3.0	67
162	Metal Ion Sensing Using Ion Chemical Exchange Saturation Transfer ¹⁹ F Magnetic Resonance Imaging. Journal of the American Chemical Society, 2013, 135, 12164-12167.	13.7	67

#	Article	IF	CITATIONS
163	Age-related changes in anterior cingulate cortex glutamate in schizophrenia: A 1H MRS Study at 7Tesla. Schizophrenia Research, 2016, 172, 101-105.	2.0	67
164	Brain and retinal atrophy in African-Americans versus Caucasian-Americans with multiple sclerosis: a longitudinal study. Brain, 2018, 141, 3115-3129.	7.6	67
165	Human White Matter Atlas. American Journal of Psychiatry, 2007, 164, 1005-1005.	7.2	66
166	Determination of wholeâ€brain oxygen extraction fractions by fast measurement of blood <i>T</i> ₂ in the jugular vein. Magnetic Resonance in Medicine, 2011, 65, 471-479.	3.0	66
167	Quantitative analysis of brain pathology based on MRI and brain atlases—Applications for cerebral palsy. NeuroImage, 2011, 54, 1854-1861.	4.2	65
168	Hemodynamic Changes after Visual Stimulation and Breath Holding Provide Evidence for an Uncoupling of Cerebral Blood Flow and Volume from Oxygen Metabolism. Journal of Cerebral Blood Flow and Metabolism, 2009, 29, 176-185.	4.3	64
169	Human Protamine-1 as an MRI Reporter Gene Based on Chemical Exchange. ACS Chemical Biology, 2014, 9, 134-138.	3.4	64
170	Investigation of the contribution of total creatine to the CEST <i>Z</i> â€spectrum of brain using a knockout mouse model. NMR in Biomedicine, 2017, 30, e3834.	2.8	64
171	High field localized proton spectroscopy in small volumes: greatly improved localization and shimming using shielded strong gradients. Magnetic Resonance in Medicine, 1989, 10, 256-265.	3.0	63
172	Measurements of cerebral perfusion and arterial hemodynamics during visual stimulation using TURBO-TILT. Magnetic Resonance in Medicine, 2003, 50, 429-433.	3.0	63
173	Physiological origin for the BOLD poststimulus undershoot in human brain: Vascular compliance versus oxygen metabolism. Journal of Cerebral Blood Flow and Metabolism, 2011, 31, 1599-1611.	4.3	62
174	Inflowâ€based vascularâ€spaceâ€occupancy (iVASO) MRI. Magnetic Resonance in Medicine, 2011, 66, 40-56.	3.0	62
175	Label-free in vivo molecular imaging of underglycosylated mucin-1 expression in tumour cells. Nature Communications, 2015, 6, 6719.	12.8	62
176	Size-Induced Enhancement of Chemical Exchange Saturation Transfer (CEST) Contrast in Liposomes. Journal of the American Chemical Society, 2008, 130, 5178-5184.	13.7	61
177	Correlation of rapid changes in the average water diffusion constant and the concentrations of lactate and ATP breakdown products during global ischemia in cat brain. Magnetic Resonance in Medicine, 1995, 34, 343-352.	3.0	60
178	Noninvasive functional imaging of cerebral blood volume with vascularâ€spaceâ€occupancy (VASO) MRI. NMR in Biomedicine, 2013, 26, 932-948.	2.8	60
179	Altered <scp>d</scp> -glucose in brain parenchyma and cerebrospinal fluid of early Alzheimer's disease detected by dynamic glucose-enhanced MRI. Science Advances, 2020, 6, eaba3884.	10.3	60
180	Reproducibility of tractâ€specific magnetization transfer and diffusion tensor imaging in the cervical spinal cord at 3 tesla. NMR in Biomedicine, 2010, 23, 207-217.	2.8	59

#	Article	IF	CITATIONS
181	Susceptibility tensor imaging (STI) of the brain. NMR in Biomedicine, 2017, 30, e3540.	2.8	59
182	Magnetic Resonance Spectroscopy and Spectroscopic Imaging for the Study of Brain Metabolism. Annals of the New York Academy of Sciences, 1997, 820, 75-96.	3.8	58
183	Unique patterns of diffusion directionality in rat brain tumors revealed by highâ€resolution diffusion tensor MRI. Magnetic Resonance in Medicine, 2007, 58, 454-462.	3.0	58
184	A dextran-based probe for the targeted magnetic resonance imaging of tumours expressing prostate-specific membrane antigen. Nature Biomedical Engineering, 2017, 1, 977-982.	22.5	58
185	High-resolution isotropic 3D diffusion tensor imaging of the human brain. Magnetic Resonance in Medicine, 2002, 47, 837-843.	3.0	57
186	Pulsed magnetization transfer imaging with body coil transmission at 3 Tesla: Feasibility and application. Magnetic Resonance in Medicine, 2006, 56, 866-875.	3.0	57
187	Water Exchange Filter (WEX Filter) for Nuclear Magnetic Resonance Studies of Macromolecules. Journal of the American Chemical Society, 1994, 116, 11982-11984.	13.7	55
188	MRI biosensor for protein kinase A encoded by a single synthetic gene. Magnetic Resonance in Medicine, 2012, 68, 1919-1923.	3.0	55
189	In vivo imaging of phosphocreatine with artificial neural networks. Nature Communications, 2020, 11, 1072.	12.8	55
190	Graded Reduction of Cerebral Blood Flow in Rat as Detected by the Nuclear Magnetic Resonance Relaxation Time T ₂ : A Theoretical and Experimental Approach. Journal of Cerebral Blood Flow and Metabolism, 2000, 20, 316-326.	4.3	54
191	Measurement of absolute arterial cerebral blood volume in human brain without using a contrast agent. NMR in Biomedicine, 2011, 24, 1313-1325.	2.8	54
192	Quantitative theory for the longitudinal relaxation time of blood water. Magnetic Resonance in Medicine, 2016, 76, 270-281.	3.0	54
193	Multi-atlas tool for automated segmentation of brain gray matter nuclei and quantification of their magnetic susceptibility. Neurolmage, 2019, 191, 337-349.	4.2	54
194	Implementation of vascularâ€spaceâ€occupancy MRI at 7T. Magnetic Resonance in Medicine, 2013, 69, 1003-1013.	3.0	52
195	A diaCEST MRI approach for monitoring liposomal accumulation in tumors. Journal of Controlled Release, 2014, 180, 51-59.	9.9	52
196	Multiple acquisitions with global inversion cycling (MAGIC): A multislice technique for vascular-space-occupancy dependent fMRI. Magnetic Resonance in Medicine, 2004, 51, 9-15.	3.0	51
197	CEST phase mapping using a length and offset varied saturation (LOVARS) scheme. Magnetic Resonance in Medicine, 2012, 68, 1074-1086.	3.0	51
198	Velocityâ€selectiveâ€inversion prepared arterial spin labeling. Magnetic Resonance in Medicine, 2016, 76, 1136-1148.	3.0	51

#	Article	IF	CITATIONS
199	NMR Study of Rapidly Exchanging Backbone Amide Protons in Staphylococcal Nuclease and the Correlation with Structural and Dynamic Properties. Journal of the American Chemical Society, 1997, 119, 6844-6852.	13.7	50
200	Protein aggregation linked to Alzheimer's disease revealed by saturation transfer MRI. NeuroImage, 2019, 188, 380-390.	4.2	50
201	Quantifying amide proton exchange rate and concentration in chemical exchange saturation transfer imaging of the human brain. NeuroImage, 2019, 189, 202-213.	4.2	50
202	Thalamic lesions in multiple sclerosis by 7T MRI: Clinical implications and relationship to cortical pathology. Multiple Sclerosis Journal, 2015, 21, 1139-1150.	3.0	49
203	CEST-MRI detects metabolite levels altered by breast cancer cell aggressiveness and chemotherapy response. NMR in Biomedicine, 2016, 29, 806-816.	2.8	49
204	CEST theranostics: label-free MR imaging of anticancer drugs. Oncotarget, 2016, 7, 6369-6378.	1.8	49
205	Intervoxel Heterogeneity of Event-Related Functional Magnetic Resonance Imaging Responses as a Function of T1 Weighting. NeuroImage, 2002, 17, 943-955.	4.2	48
206	Origin and minimization of residual motionâ€related artifacts in navigatorâ€corrected segmented diffusionâ€weighted EPI of the human brain. Magnetic Resonance in Medicine, 2002, 47, 818-822.	3.0	48
207	Suppression of lipid artifacts in amide proton transfer imaging. Magnetic Resonance in Medicine, 2005, 54, 222-225.	3.0	48
208	Evaluation of human brain tumor heterogeneity using multiple <i>T</i> ₁ â€based MRI signal weighting approaches. Magnetic Resonance in Medicine, 2008, 59, 336-344.	3.0	48
209	Quantitative magnetization transfer characteristics of the human cervical spinal cord in vivo: Application to Adrenomyeloneuropathy. Magnetic Resonance in Medicine, 2009, 61, 22-27.	3.0	48
210	Consensus statement on current and emerging methods for the diagnosis and evaluation of cerebrovascular disease. Journal of Cerebral Blood Flow and Metabolism, 2018, 38, 1391-1417.	4.3	48
211	MRI contrast-dose relationship of manganese(III)tetra(4-sulfonatophenyl) porphyrin with human xenograft tumors in nude mice at 2.0 T. Magnetic Resonance Imaging, 1992, 10, 919-928.	1.8	47
212	Detection of rapidly exchanging compounds using onâ€resonance frequencyâ€labeled exchange (FLEX) transfer. Magnetic Resonance in Medicine, 2012, 68, 1048-1055.	3.0	47
213	Elevated arteriolar cerebral blood volume in prodromal Huntington's disease. Movement Disorders, 2014, 29, 396-401.	3.9	47
214	Hematocrit and oxygenation dependence of blood ¹ H ₂ O <i>T</i> ₁ at 7 tesla. Magnetic Resonance in Medicine, 2013, 70, 1153-1159.	3.0	45
215	Carbon Dots as a New Class of Diamagnetic Chemical Exchange Saturation Transfer (diaCEST) MRI Contrast Agents. Angewandte Chemie - International Edition, 2019, 58, 9871-9875.	13.8	45
216	Altered brain iron content and deposition rate in Huntington's disease as indicated by quantitative susceptibility MRI. Journal of Neuroscience Research, 2019, 97, 467-479.	2.9	45

#	Article	IF	CITATIONS
217	Measurement of water–amide proton exchange rates in the denatured state of staphylococcal nuclease by a magnetization transfer technique. Proteins: Structure, Function and Bioinformatics, 1997, 28, 325-332.	2.6	44
218	Stem cell profiling by nuclear magnetic resonance spectroscopy. Magnetic Resonance in Medicine, 2006, 56, 666-670.	3.0	44
219	A review of the development of Vascular-Space-Occupancy (VASO) fMRI. NeuroImage, 2012, 62, 736-742.	4.2	44
220	Imaging meningeal inflammation in CNS autoimmunity identifies a therapeutic role for BTK inhibition. Brain, 2021, 144, 1396-1408.	7.6	44
221	<i>q</i> â€space and conventional diffusion imaging of axon and myelin damage in the rat spinal cord after axotomy. Magnetic Resonance in Medicine, 2010, 63, 1323-1335.	3.0	43
222	Extensive neurological recovery from a complete spinal cord injury: a case report and hypothesis on the role of cortical plasticity. Frontiers in Human Neuroscience, 2013, 7, 290.	2.0	43
223	Tuning Phenols with Intraâ€Molecular Bond Shifted HYdrogens (IMâ€SHY) as diaCEST MRI Contrast Agents. Chemistry - A European Journal, 2014, 20, 15824-15832.	3.3	43
224	Memory performance-related dynamic brain connectivity indicates pathological burden and genetic risk for Alzheimer's disease. Alzheimer's Research and Therapy, 2017, 9, 24.	6.2	43
225	Fast measurement of blood T ₁ in the human carotid artery at 3T: Accuracy, precision, and reproducibility. Magnetic Resonance in Medicine, 2017, 77, 2296-2302.	3.0	43
226	Highly efficient magnetic labelling allows MRI tracking of the homing of stem cellâ€derived extracellular vesicles following systemic delivery. Journal of Extracellular Vesicles, 2021, 10, e12054.	12.2	43
227	InverseT2 contrast at 1.5 Tesla between gray matter and white matter in the occipital lobe of normal adult human brain. Magnetic Resonance in Medicine, 2001, 46, 401-406.	3.0	42
228	Magnetization transfer weighted imaging in the upper cervical spinal cord using cerebrospinal fluid as intersubject normalization reference (MTCSF imaging). Magnetic Resonance in Medicine, 2005, 54, 201-206.	3.0	42
229	Direct saturation MRI: Theory and application to imaging brain iron. Magnetic Resonance in Medicine, 2009, 62, 384-393.	3.0	42
230	CEST MRI of 3â€Oâ€methylâ€Dâ€glucose uptake and accumulation in brain tumors. Magnetic Resonance in Medicine, 2019, 81, 1993-2000.	3.0	42
231	<scp>d</scp> â€glucose weighted chemical exchange saturation transfer (glucoCEST)â€based dynamic glucose enhanced (DGE) MRI at 3T: early experience in healthy volunteers and brain tumor patients. Magnetic Resonance in Medicine, 2020, 84, 247-262.	3.0	41
232	Magnetic resonance imaging of glycogen using its magnetic coupling with water. Proceedings of the National Academy of Sciences of the United States of America, 2020, 117, 3144-3149.	7.1	41
233	Scan time reduction in proton magnetic resonance spectroscopic imaging of the human brain. Magnetic Resonance in Medicine, 2002, 47, 384-387.	3.0	40
234	Multi-Modal MRI Analysis with Disease-Specific Spatial Filtering: Initial Testing to Predict Mild Cognitive Impairment Patients Who Convert to Alzheimer?s Disease. Frontiers in Neurology, 2011, 2, 54.	2.4	40

#	Article	IF	CITATIONS
235	Magnetic Resonance Diffusion Tensor Microimaging Reveals a Role for Bcl-x in Brain Development and Homeostasis. Journal of Neuroscience, 2005, 25, 1881-1888.	3.6	39
236	Noninvasive imaging of infection after treatment with tumorâ€homing bacteria using Chemical Exchange Saturation Transfer (CEST) MRI. Magnetic Resonance in Medicine, 2013, 70, 1690-1698.	3.0	39
237	Wholeâ€brain threeâ€dimensional T2â€weighted BOLD functional magnetic resonance imaging at 7 Tesla. Magnetic Resonance in Medicine, 2014, 72, 1530-1540.	3.0	39
238	Association of cerebrovascular reactivity and Alzheimer pathologic markers with cognitive performance. Neurology, 2020, 95, e962-e972.	1.1	39
239	FAIR excluding radiation damping (FAIRER). Magnetic Resonance in Medicine, 1998, 40, 712-719.	3.0	38
240	Altered functional connectivity between sub-regions in the thalamus and cortex in schizophrenia patients measured by resting state BOLD fMRI at 7T. Schizophrenia Research, 2019, 206, 370-377.	2.0	38
241	Superficially Located White Matter Structures Commonly Seen in the Human and the Macaque Brain with Diffusion Tensor Imaging. Brain Connectivity, 2011, 1, 37-47.	1.7	37
242	Localized diffusion magnetic resonance micro-imaging of the live mouse brain. NeuroImage, 2014, 91, 12-20.	4.2	37
243	Quantitative Susceptibility Mapping Using Structural Feature Based Collaborative Reconstruction Pub _newline ? (SFCR) in the Human Brain. IEEE Transactions on Medical Imaging, 2016, 35, 2040-2050.	8.9	37
244	In situ changes in purine nucleotide and n-acetyl concentrations upon inducing global ischemia in cat brain. Magnetic Resonance in Medicine, 1993, 29, 381-385.	3.0	36
245	Fast measurement of blood <i>T</i> ₁ in the human jugular vein at 3 Tesla. Magnetic Resonance in Medicine, 2011, 65, 1297-1304.	3.0	36
246	Threeâ€dimensional wholeâ€brain perfusion quantification using pseudoâ€continuous arterial spin labeling MRI at multiple postâ€labeling delays: accounting for both arterial transit time and impulse response function. NMR in Biomedicine, 2014, 27, 116-128.	2.8	35
247	Onâ€resonance variable delay multipulse scheme for imaging of fastâ€exchanging protons and semisolid macromolecules. Magnetic Resonance in Medicine, 2017, 77, 730-739.	3.0	35
248	Single-shot localized echo-planar imaging (STEAM-EPI) at 4.7 tesla. Magnetic Resonance in Medicine, 1990, 14, 401-408.	3.0	34
249	Information from combined 1H and 31P NMR studies of cell extracts: Differences in metabolism between drug-sensitive and drug-resistant MCF-7 human breast cancer cells. Biochemical and Biophysical Research Communications, 1990, 169, 383-390.	2.1	34
250	Reliability and reproducibility of perfusion MRI in cognitively normal subjects. Magnetic Resonance Imaging, 2010, 28, 1283-1289.	1.8	34
251	Separating fast and slow exchange transfer and magnetization transfer using offâ€resonance variableâ€delay multipleâ€pulse (VDMP) MRI. Magnetic Resonance in Medicine, 2018, 80, 1568-1576.	3.0	34
252	Feasibility of concurrent dual contrast enhancement using CEST contrast agents and superparamagnetic iron oxide particles. Magnetic Resonance in Medicine, 2009, 61, 970-974.	3.0	33

#	Article	IF	CITATIONS
253	Non-invasive temperature mapping using temperature-responsive water saturation shift referencing (T-WASSR) MRI. NMR in Biomedicine, 2014, 27, 320-331.	2.8	33
254	Characterization of tumor vascular permeability using natural dextrans and CEST MRI. Magnetic Resonance in Medicine, 2018, 79, 1001-1009.	3.0	33
255	Pulseq EST: Towards multiâ€site multiâ€vendor compatibility and reproducibility of CEST experiments using an openâ€source sequence standard. Magnetic Resonance in Medicine, 2021, 86, 1845-1858.	3.0	33
256	Imaging of shifted stimulated echoes and multiple spin echoes. Magnetic Resonance in Medicine, 1997, 37, 336-340.	3.0	32
257	Rapid threeâ€dimensional diffusion MRI facilitates the study of acute stroke in mice. Magnetic Resonance in Medicine, 2001, 46, 183-188.	3.0	32
258	MR diffusion tensor imaging documented arcuate fasciculus lesion in a patient with normal repetition performance. Aphasiology, 2002, 16, 897-902.	2.2	32
259	Magnetization transfer enhanced vascularâ€spaceâ€occupancy (MTâ€VASO) functional MRI. Magnetic Resonance in Medicine, 2009, 61, 944-951.	3.0	31
260	Prefrontal executive function associated coupling relates to Huntington's disease stage. Cortex, 2013, 49, 2661-2673.	2.4	31
261	Wholeâ€brain arteriography and venography: Using improved velocityâ€selective saturation pulse trains. Magnetic Resonance in Medicine, 2018, 79, 2014-2023.	3.0	31
262	Quantitative theory for the transverse relaxation time of blood water. NMR in Biomedicine, 2020, 33, e4207.	2.8	31
263	Torsional angles in vinylarenes determined by high-field NMR spectroscopy. Journal of the American Chemical Society, 1988, 110, 4900-4905.	13.7	29
264	In Vivo Determination of Absolute Cerebral Blood Volume Using Hemoglobin as a Natural Contrast Agent: An MRI Study Using Altered Arterial Carbon Dioxide Tension. Journal of Cerebral Blood Flow and Metabolism, 1999, 19, 809-817.	4.3	29
265	Effect of inflow of fresh blood on vascularâ€spaceâ€occupancy (VASO) contrast. Magnetic Resonance in Medicine, 2009, 61, 473-480.	3.0	29
266	Accounting for the role of hematocrit in betweenâ€subject variations of MRIâ€derived baseline cerebral hemodynamic parameters and functional BOLD responses. Human Brain Mapping, 2018, 39, 344-353.	3.6	29
267	Highâ€resolution creatine mapping of mouse brain at 11.7 T using nonâ€steadyâ€state chemical exchange saturation transfer. NMR in Biomedicine, 2019, 32, e4168.	2.8	29
268	Quantitative Susceptibility Mapping of Brain Iron and Î ² -Amyloid in MRI and PET Relating to Cognitive Performance in Cognitively Normal Older Adults. Radiology, 2021, 298, 353-362.	7.3	29
269	Abnormal Grey Matter Arteriolar Cerebral Blood Volume in Schizophrenia Measured With 3D Inflow-Based Vascular-Space-Occupancy MRI at 7T. Schizophrenia Bulletin, 2017, 43, sbw109.	4.3	28
270	CEST MRI of sepsisâ€induced acute kidney injury. NMR in Biomedicine, 2018, 31, e3942.	2.8	28

#	Article	IF	CITATIONS
271	Quantification of wholeâ€brain oxygenation extraction fraction and cerebral metabolic rate of oxygen consumption in adults with sickle cell anemia using individual T ₂ â€based oxygenation calibrations. Magnetic Resonance in Medicine, 2020, 83, 1066-1080.	3.0	28
272	Gradient-enhanced 3D NOESY-HMQC spectroscopy. Journal of Biomolecular NMR, 1992, 2, 301-305.	2.8	27
273	Correction of motional artifacts in diffusion-weighted images using a reference phase map. Magnetic Resonance in Medicine, 1995, 34, 476-480.	3.0	27
274	Mean magnetic susceptibility regularized susceptibility tensor imaging (<scp>MMSR</scp> â€ <scp>STI</scp>) for estimating orientations of white matter fibers in human brain. Magnetic Resonance in Medicine, 2014, 72, 610-619.	3.0	27
275	Multiâ€echo Length and Offset VARied Saturation (MeLOVARS) method for improved CEST imaging. Magnetic Resonance in Medicine, 2015, 73, 488-496.	3.0	27
276	Detection and Quantification of Hydrogen Peroxide in Aqueous Solutions Using Chemical Exchange Saturation Transfer. Analytical Chemistry, 2017, 89, 7758-7764.	6.5	27
277	D-Glucose uptake and clearance in the tauopathy Alzheimer's disease mouse brain detected by on-resonance variable delay multiple pulse MRI. Journal of Cerebral Blood Flow and Metabolism, 2021, 41, 1013-1025.	4.3	27
278	Effect of transit times on quantification of cerebral blood flow by the FAIR T1-difference approach. Magnetic Resonance in Medicine, 1999, 42, 890-894.	3.0	26
279	Landmark-referenced voxel-based analysis of diffusion tensor images of the brainstem white matter tracts. NeuroImage, 2009, 44, 906-913.	4.2	26
280	Transverse water relaxation in whole blood and erythrocytes at 3T, 7T, 9.4T, 11.7T and 16.4T; determination of intracellular hemoglobin and extracellular albumin relaxivities. Magnetic Resonance Imaging, 2017, 38, 234-249.	1.8	26
281	GlucoCEST imaging with onâ€resonance variable delay multiple pulse (onVDMP) MRI. Magnetic Resonance in Medicine, 2019, 81, 47-56.	3.0	26
282	Wholeâ€brain amide CEST imaging at 3T with a steadyâ€state radial MRI acquisition. Magnetic Resonance in Medicine, 2021, 86, 893-906.	3.0	26
283	Optimized Excitation and Automation for High-Resolution NMR UsingB1-Insensitive Rotation Pulses. Journal of the American Chemical Society, 1996, 118, 5510-5511.	13.7	25
284	Multiple tuning of birdcage resonators. Magnetic Resonance in Medicine, 1997, 37, 243-251.	3.0	25
285	Imaging of Endogenous Exchangeable Proton Signals in the Human Brain Using Frequency Labeled Exchange Transfer Imaging. Magnetic Resonance in Medicine, 2013, 69, 966-973.	3.0	25
286	MRI detection of bacterial brain abscesses and monitoring of antibiotic treatment using bacCEST. Magnetic Resonance in Medicine, 2018, 80, 662-671.	3.0	25
287	Low cortical iron and high entorhinal cortex volume promote cognitive functioning in the oldest-old. Neurobiology of Aging, 2018, 64, 68-75.	3.1	25
288	CEST, ASL, and magnetization transfer contrast: How similar pulse sequences detect different phenomena. Magnetic Resonance in Medicine, 2018, 80, 1320-1340.	3.0	25

#	Article	IF	CITATIONS
289	Prospective acceleration of parallel RF transmissionâ€based 3D chemical exchange saturation transfer imaging with compressed sensing. Magnetic Resonance in Medicine, 2019, 82, 1812-1821.	3.0	25
290	Extradomain-B Fibronectin-Targeted Dextran-Based Chemical Exchange Saturation Transfer Magnetic Resonance Imaging Probe for Detecting Pancreatic Cancer. Bioconjugate Chemistry, 2019, 30, 1425-1433.	3.6	25
291	Arterial Input Functions and Tissue Response Curves in Dynamic Glucose-Enhanced (DGE) Imaging: Comparison between glucoCEST and Blood Glucose Sampling in Humans. Tomography, 2018, 4, 164-171.	1.8	25
292	Single-shot diffusion-weighted trace imaging on a clinical scanner. Magnetic Resonance in Medicine, 1998, 40, 622-628.	3.0	24
293	Vascular space occupancy (VASO) cerebral blood volumeâ€weighted MRI identifies hemodynamic impairment in patients with carotid artery disease. Journal of Magnetic Resonance Imaging, 2009, 29, 718-724.	3.4	24
294	CT and CEST MRI bimodal imaging of the intratumoral distribution of iodinated liposomes. Quantitative Imaging in Medicine and Surgery, 2019, 9, 1579-1591.	2.0	24
295	Highâ€sensitivity CEST mapping using a spatiotemporal correlationâ€enhanced method. Magnetic Resonance in Medicine, 2020, 84, 3342-3350.	3.0	24
296	NMR studies of brain 13C-glucose uptake and metabolism: Present status. Magnetic Resonance Imaging, 1995, 13, 1213-1221.	1.8	23
297	Study of the Spatial Correlation Between Neuronal Activity and BOLD fMRI Responses Evoked by Sensory and Channelrhodopsin-2 Stimulation in the Rat Somatosensory Cortex. Journal of Molecular Neuroscience, 2014, 53, 553-61.	2.3	23
298	Cerebral blood volume mapping using Fourierâ€transform–based velocityâ€selective saturation pulse trains. Magnetic Resonance in Medicine, 2019, 81, 3544-3554.	3.0	23
299	APOE4 moderates effects of cortical iron on synchronized default mode network activity in cognitively healthy oldâ€aged adults. Alzheimer's and Dementia: Diagnosis, Assessment and Disease Monitoring, 2020, 12, e12002.	2.4	23
300	Proton magnetic resonance spectroscopy of small regions (1 mL) localized inside superficial human tumors. A clinical feasibility study. NMR in Biomedicine, 1990, 3, 227-232.	2.8	22
301	Quantitative measurement of cerebral blood volume using velocityâ€selective pulse trains. Magnetic Resonance in Medicine, 2017, 77, 92-101.	3.0	22
302	Using the water signal to detect invisible exchanging protons in the catalytic triad of a serine protease. Journal of Biomolecular NMR, 2011, 50, 299-314.	2.8	21
303	Using frequencyâ€labeled exchange transfer to separate out conventional magnetization transfer effects from exchange transfer effects when detecting ParaCEST agents. Magnetic Resonance in Medicine, 2012, 67, 906-911.	3.0	21
304	Screening CEST contrast agents using ultrafast CEST imaging. Journal of Magnetic Resonance, 2016, 265, 224-229.	2.1	21
305	ClucoCEST magnetic resonance imaging inÂvivo may be diagnostic of acute renal allograft rejection. Kidney International, 2017, 92, 757-764.	5.2	21
306	Huntingtin silencing delays onset and slows progression of Huntington's disease: a biomarker study. Brain, 2021, 144, 3101-3113.	7.6	21

#	Article	IF	CITATIONS
307	Intervoxel heterogeneity of event-related functional magnetic resonance imaging responses as a function of T(1) weighting. NeuroImage, 2002, 17, 943-55.	4.2	21
308	Image contrast using the secondary and tertiary eigenvectors in diffusion tensor imaging. Magnetic Resonance in Medicine, 2006, 55, 439-449.	3.0	20
309	Advanced MRI strategies for assessing spinal cord injury. Handbook of Clinical Neurology / Edited By P J Vinken and G W Bruyn, 2012, 109, 85-101.	1.8	20
310	Early detection of Alzheimer's disease using creatine chemical exchange saturation transfer magnetic resonance imaging. NeuroImage, 2021, 236, 118071.	4.2	20
311	Measurement of parenchymal extravascular <i>R</i> ₂ * and tissue oxygen extraction fraction using multiâ€echo vascular space occupancy MRI at 7 T. NMR in Biomedicine, 2015, 28, 264-271.	2.8	19
312	Susceptibilityâ€based analysis of dynamic gadolinium bolus perfusion MRI. Magnetic Resonance in Medicine, 2015, 73, 544-554.	3.0	19
313	Biophysical Characterization of Human Protamine-1 as a Responsive CEST MR Contrast Agent. ACS Macro Letters, 2015, 4, 34-38.	4.8	19
314	Differential Changes in Functional Connectivity of Striatum-Prefrontal and Striatum-Motor Circuits in Premanifest Huntington's Disease. Neurodegenerative Diseases, 2019, 19, 78-87.	1.4	19
315	Retinotopic mapping in the human visual cortex using vascular space occupancy-dependent functional magnetic resonance imaging. NeuroReport, 2005, 16, 1635-1640.	1.2	18
316	Detection of dynamic substrate binding using MRI. Scientific Reports, 2017, 7, 10138.	3.3	18
317	CEST MRI monitoring of tumor response to vascular disrupting therapy using high molecular weight dextrans. Magnetic Resonance in Medicine, 2019, 82, 1471-1479.	3.0	18
318	Quantitative magnetic susceptibility mapping without phase unwrapping using WASSR. NeuroImage, 2014, 86, 265-279.	4.2	17
319	Hyperpolarized MRI, functional MRI, MR spectroscopy and CEST to provide metabolic information inÁvivo. Current Opinion in Chemical Biology, 2021, 63, 209-218.	6.1	17
320	Perfusion imaging using FAIR with a short predelay. Magnetic Resonance in Medicine, 1999, 41, 1099-1107.	3.0	16
321	NOrmalized MAgnetization Ratio (NOMAR) filtering for creation of tissue selective contrast maps. Magnetic Resonance in Medicine, 2013, 69, 516-523.	3.0	16
322	Magnetization transfer contrast MRI for non-invasive assessment of innate and adaptive immune responses against alginate-encapsulated cells. Biomaterials, 2014, 35, 7811-7818.	11.4	16
323	¹⁵ N Heteronuclear Chemical Exchange Saturation Transfer MRI. Journal of the American Chemical Society, 2016, 138, 11136-11139.	13.7	16
324	Diffusion-regularized susceptibility tensor imaging (DRSTI) of tissue microstructures in the human brain. Medical Image Analysis, 2021, 67, 101827.	11.6	16

#	Article	IF	CITATIONS
325	Visual Activation in α-Chloralose-anaesthetized Cats Does Not Cause Lactate Accumulation in the Visual Cortex as Detected by [1HINMR Difference Spectroscopy. European Journal of Neuroscience, 1997, 9, 654-661.	2.6	15
326	Magnetic resonance microscopy and histology of the CNS. Trends in Biotechnology, 2002, 20, S24-S28.	9.3	14
327	Learned Proximal Networks for Quantitative Susceptibility Mapping. Lecture Notes in Computer Science, 2020, 12262, 125-135.	1.3	14
328	Measurement of arteriolar blood volume in brain tumors using MRI without exogenous contrast agent administration at 7T. Journal of Magnetic Resonance Imaging, 2016, 44, 1244-1255.	3.4	13
329	Detecting acid phosphatase enzymatic activity with phenol as a chemical exchange saturation transfer magnetic resonance imaging contrast agent (PhenolCEST MRI). Biosensors and Bioelectronics, 2019, 141, 111442.	10.1	13
330	Extracellular vesicles reveal abnormalities in neuronal iron metabolism in restless legs syndrome. Sleep, 2019, 42, .	1.1	13
331	The effect of the mTOR inhibitor rapamycin on glucoCEST signal in a preclinical model of glioblastoma. Magnetic Resonance in Medicine, 2019, 81, 3798-3807.	3.0	13
332	Age-Related Alterations in Brain Perfusion, Venous Oxygenation, and Oxygen Metabolic Rate of Mice: A 17-Month Longitudinal MRI Study. Frontiers in Neurology, 2020, 11, 559.	2.4	13
333	Background field removal using a region adaptive kernel for quantitative susceptibility mapping of human brain. Journal of Magnetic Resonance, 2017, 281, 130-140.	2.1	12
334	Molecular imaging of deoxycytidine kinase activity using deoxycytidine-enhanced CEST MRI. Cancer Research, 2019, 79, canres.3565.2018.	0.9	12
335	Background field removal for susceptibility mapping of human brain with large susceptibility variations. Magnetic Resonance in Medicine, 2019, 81, 2025-2037.	3.0	12
336	Whole-Brain Functional and Diffusion Tensor MRI in Human Participants with Metallic Orthodontic Braces. Radiology, 2020, 294, 149-157.	7.3	12
337	Fast whole brain MR imaging of dynamic susceptibility contrast changes in the cerebrospinal fluid (cDSC MRI). Magnetic Resonance in Medicine, 2020, 84, 3256-3270.	3.0	12
338	Mechanism and quantitative assessment of saturation transfer for waterâ€based detection of the aliphatic protons in carbohydrate polymers. Magnetic Resonance in Medicine, 2021, 85, 1643-1654.	3.0	12
339	Threeâ€dimensional wholeâ€brain mapping of cerebral blood volume and venous cerebral blood volume using Fourier transform–based velocityâ€selective pulse trains. Magnetic Resonance in Medicine, 2021, 86, 1420-1433.	3.0	12
340	Assessment of Amide proton transfer weighted (APTw) MRI for pre-surgical prediction of final diagnosis in gliomas. PLoS ONE, 2020, 15, e0244003.	2.5	12
341	Deep learningâ€based classification of preclinical breast cancer tumor models using chemical exchange saturation transfer magnetic resonance imaging. NMR in Biomedicine, 2022, 35, e4626.	2.8	12
342	Measurement of cerebral blood flow by volumeâ€selective 19 F NMR spectroscopy. Magnetic Resonance in Medicine, 1990, 16, 489-495.	3.0	11

#	Article	IF	CITATIONS
343	Time domain removal of irrelevant magnetization in chemical exchange saturation transfer Zâ€spectra. Magnetic Resonance in Medicine, 2013, 70, 547-555.	3.0	11
344	Salicylic Acidâ€Based Polymeric Contrast Agents for Molecular Magnetic Resonance Imaging of Prostate Cancer. Chemistry - A European Journal, 2018, 24, 7235-7242.	3.3	11
345	Quantitative assessment of cerebral venous blood T ₂ in mouse at 11.7T: Implementation, optimization, and age effect. Magnetic Resonance in Medicine, 2018, 80, 521-528.	3.0	11
346	Optimization of phase ontrast MRI for the estimation of global cerebral blood flow of mice at 11.7T. Magnetic Resonance in Medicine, 2019, 81, 2566-2575.	3.0	11
347	Three-dimensional tracking of axonal projections in the brain by magnetic resonance imaging. , 1999, 45, 265.		11
348	Gross feature recognition of Anatomical Images based on Atlas grid (GAIA): Incorporating the local discrepancy between an atlas and a target image to capture the features of anatomic brain MRI. NeuroImage: Clinical, 2013, 3, 202-211.	2.7	10
349	In vivo imaging of paraCEST agents using frequency labeled exchange transfer <scp>MRI</scp> . Magnetic Resonance in Medicine, 2014, 71, 286-293.	3.0	10
350	Steady pulsed imaging and labeling scheme for noninvasive perfusion imaging. Magnetic Resonance in Medicine, 2016, 75, 238-248.	3.0	10
351	In vivo magnetic resonance imaging and spectroscopy. Technological advances and opportunities for applications continue to abound. Journal of Magnetic Resonance, 2019, 306, 55-65.	2.1	10
352	Increased cerebral blood volume in small arterial vessels is aÂcorrelate of amyloid-β–related cognitive decline. Neurobiology of Aging, 2019, 76, 181-193.	3.1	10
353	Monitoring diffuse injury during disease progression in experimental autoimmune encephalomyelitis with on resonance variable delay multiple pulse (onVDMP) CEST MRI. NeuroImage, 2020, 204, 116245.	4.2	10
354	Language Mapping Using T2-Prepared BOLD Functional MRI in the Presence of Large Susceptibility Artifacts—Initial Results in Patients With Brain Tumor and Epilepsy. Tomography, 2017, 3, 105-113.	1.8	9
355	Diffuse Abnormality of Low to Moderately Organized White Matter in Schizophrenia. Brain Connectivity, 2011, 1, 511-519.	1.7	8
356	A three-dimensional single-scan approach for the measurement of changes in cerebral blood volume, blood flow, and blood oxygenation-weighted signals during functional stimulation. NeuroImage, 2017, 147, 976-984.	4.2	8
357	Subject-specific regional measures of water diffusion are associated with impairment in chronic spinal cord injury. Neuroradiology, 2017, 59, 747-758.	2.2	7
358	MTT and Blood-Brain Barrier Disruption within Asymptomatic Vascular WM Lesions. American Journal of Neuroradiology, 2021, 42, 1396-1402.	2.4	7
359	Towards robust glucose chemical exchange saturation transfer imaging in humans at 3ÂT: Arterial input function measurements and the effects of infusion time. NMR in Biomedicine, 2022, 35, e4624.	2.8	7
360	Functional Activities Detected in the Olfactory Bulb and Associated Olfactory Regions in the Human Brain Using T2-Prepared BOLD Functional MRI at 7T. Frontiers in Neuroscience, 2021, 15, 723441.	2.8	7

#	Article	IF	CITATIONS
361	Deuterium oxide as a contrast medium for real-time MRI-guided endovascular neurointervention. Theranostics, 2021, 11, 6240-6250.	10.0	7
362	Dynamic contrastâ€enhanced CEST MRI using a low molecular weight dextran. NMR in Biomedicine, 2021, , e4649.	2.8	7
363	<scp>T₂â€oximetry–</scp> based cerebral venous oxygenation mapping using <scp>Fourierâ€transform</scp> –based <scp>velocityâ€selective</scp> pulse trains. Magnetic Resonance in Medicine, 2022, 88, 1292-1302.	3.0	7
364	A framework on surface-based connectivity quantification for the human brain. Journal of Neuroscience Methods, 2011, 197, 324-332.	2.5	6
365	Molecular Imaging of CXCL12 Promoter-driven HSV1-TK Reporter Gene Expression. Biotechnology and Bioprocess Engineering, 2018, 23, 208-217.	2.6	6
366	Five-year longitudinal changes in quantitative spinal cord MRI in multiple sclerosis. Multiple Sclerosis Journal, 2021, 27, 549-558.	3.0	6
367	High field NMR, a powerful new analytical tool. TrAC - Trends in Analytical Chemistry, 1987, 6, 23-26.	11.4	5
368	Impaired response of cerebral oxygen metabolism to visual stimulation in Huntington's disease. Journal of Cerebral Blood Flow and Metabolism, 2021, 41, 1119-1130.	4.3	5
369	Detection of electrostatic molecular binding using the water proton signal. Magnetic Resonance in Medicine, 2022, 88, 901-915.	3.0	5
370	Three-dimensional acquisition of cerebral blood volume and flow responses during functional stimulation in a single scan. NeuroImage, 2014, 103, 533-541.	4.2	4
371	Spectroscopic measurements of metabolic fluxes. Nature Biomedical Engineering, 2020, 4, 254-256.	22.5	3
372	Singleâ€step calculation of susceptibility through multiple orientation sampling. NMR in Biomedicine, 2021, 34, e4517.	2.8	3
373	APT-weighted MRI Can Be an Early Marker for Demyelination. Radiology, 2021, 299, 435-437.	7.3	3
374	Quantitative magnetic resonance imaging assessment of cerebral ischemia in rat using onâ€resonance T1 in the rotating frame. Magnetic Resonance in Medicine, 1999, 42, 268-276.	3.0	3
375	Dynamic Susceptibility Contrast MRI at 7 T: Tail-Scaling Analysis and Inferences about Field Strength Dependence. Tomography, 2017, 3, 74-78.	1.8	3
376	Measurement of water–amide proton exchange rates in the denatured state of staphylococcal nuclease by a magnetization transfer technique. Proteins: Structure, Function and Bioinformatics, 1997, 28, 325-332.	2.6	2
377	Quantitative proton MR spectroscopic imaging of normal human cerebellum and brain stem. Magnetic Resonance in Medicine, 2001, 46, 699-705.	3.0	2
378	Ultra-high-field (7.0 Tesla and above) MRI is now necessary to make the next step forward in understanding MS pathophysiology – Commentary. Multiple Sclerosis Journal, 2017, 23, 376-377.	3.0	1

#	Article	IF	CITATIONS
379	Mutant G2019S-LRRK2 Induces Abnormalities in Arteriolar Cerebral Blood Volume in Mouse Brains: An MRI Study. Neurodegenerative Diseases, 2020, 20, 65-72.	1.4	1
380	In vivo visualization of human neural pathways by magnetic resonance imaging. , 2000, 47, 412.		1
381	Characterization of Mouse Brain and Its Development using Diffusion Tensor Imaging and Computational Techniques. Annual International Conference of the IEEE Engineering in Medicine and Biology Society, 2006, , .	0.5	1
382	CEST MRI and MALDI imaging reveal metabolic alterations in the cervical lymph nodes of EAE mice. Journal of Neuroinflammation, 2022, 19, .	7.2	1
383	CO2 cerebrovascular reactivity measured with phaseâ€contrast MRI: A potential biomarker of cognition and physical function in older adults. Alzheimer's and Dementia, 2020, 16, e042215.	0.8	Ο
384	CEST (Chemical Exchange Saturation Transfer) MR Molecular Imaging. , 2021, , 325-341.		0
385	Resolution and inversion time dependence of CBF measurements using MRI: A possible explanation for discrepancy between MRI and PET. Journal of Cerebral Blood Flow and Metabolism, 2005, 25, S320-S320.	4.3	Ο
386	Alternative Methods for fMRI. Biological Magnetic Resonance, 2015, , 271-309.	0.4	0
387	Chapter 6 General Theory of CEST Image Acquisition and Post-Processing. , 2017, , 55-96.		Ο
388	Chapter 3 History of In Vivo Exchange Transfer Spectroscopy and Imaging in Baltimore. , 2017, , 17-38.		0